EurJIC
European Journal of Inorganic Chemistry

A Journal of ChemPubSoc Europe

Accepted Article

Title: Histaminol and its complexes with copper(II) - studies in solid state and solution

Authors: Piotr Maślewski, Dariusz Wyrzykowski, Maciej Witwicki, and Anna Dołęga

To be cited as: *Eur. J. Inorg. Chem.* 10.1002/ejic.201701411

Link to VoR: http://dx.doi.org/10.1002/ejic.201701411

WILEY-VCH

10.1002/ejic.201701411

WILEY-VCH

Histaminol and its complexes with copper(II) – studies in solid state and solution

Piotr Maślewski[a], Dariusz Wyrzykowski[b], Maciej Witwicki[c], Anna Dołęga*[a]

Dedicated to Professor JuliaJezierska on the occasion of her 70th birthday

Abstract: Histaminol (4(5)-(β-hydroxyethyl)imidazole, 4-(1H-Imidazol-2-yl)ethanol, **L**) is an analogue of histamine and its minor metabolite. So far its properties have not been studied in detail due to the synthetic difficulties. Here the structure and acid-base properties of histaminol as well as the results of studies on its copper(II) complexes in solid state and aqueous solution are reported. Stability constants of the histaminol - Cu(II) system are measured and each stage of the complex formation is illustrated with the relevant crystal structure and the EPR spectrum.

Introduction

Histamine is a mediator of allergic and inflammatory reactions, the immune response and neuro transmission in brain, which commonly occurs in various human tissues. It is synthesized from amino acid L-histidine by the L-histidine decarboxylase enzyme (HDC). This biogenic amine is produced and stored in the mast cells and basophils. It is also secreted by T lymphocytes, thrombocytes and dendrites.[1-3] Histamine has a very wide physiological role in the human organism: it takes part in the regulation of sleep, blood pressure, gastric acid secretion, vasodilatation process and heart stimulation.[1-6]

There are two main pathways of histamine metabolism in the human body. Products of the first of them are N-methylhistamine and N-methylimidazole acetic acid. Enzymes responsible for the metabolism are histamine N-methyltransferase and monoamine oxidase (MAO). In the second pathway diamine oxidase (DAO) converts histamine to imidazole acetaldehyde, which is later metabolized to imidazole acetic acid, imidazole acetic acid riboside and finally to histaminol, a compound that is a “hero” of this paper.[2,3,7]

Histaminol (4(5)-(β-hydroxyethyl)imidazole) is an analogue of histamine and its minor metabolite. In the human urine histaminol represents about 2% of all histamine metabolites.[7] It is also a weak inhibitor of diamine oxidase enzyme.[8] Furthermore histaminol was identified as a component of wine. During alcoholic fermentation yeasts of Saccharomyces genus transform amino acids into alcohols through Ehrlich pathway. Therefore histaminol is a product of their catabolism of histidine.[8,9] Some mycobacteria species were reported to oxidize histamine to histaminol (*M. diernhoferi, M. fortuitum, M. chelonei*).[10]

Due to the synthetic difficulties the chemistry of histaminol has been relatively poorly studied. Here we report the structure and acid-base properties of histaminol as well as the results of studies on its copper(II) complexes in solid state and aqueous solution. Copper was selected as a metal ion that forms fairly stable Cu(II)-imidazole complexes, especially in the physiological pH range. Copper ions are present in almost all cells in the human body, with the highest concentration in brain, liver and heart. Copper proteins that participate in the electron transfer and several redox (oxidation) reactions, possess at least one histidine moiety in the metal binding site.[11-14] Formation of complexes with transition metal ions, such as Cu(II), Ni(II), Zn(II), Co(II), may influence the pharmacological effects of histamine and its congeners. Moreover, the activity of some anti-histamine compounds relies on their competition with histamine for binding receptor sites, which, in some cases, involve transition metal ions.[15-18] We have therefore measured stability constants of the histaminol - Cu(II) system and illustrated almost each stage of the complex formation with the relevant crystal structure and EPR spectrum.

Results and Discussion

Syntheses

The syntheses of the crystalline form of the complexes were rather simple as described in the experimental part. The synthesis of histaminol was challenging especially taking into account the necessary decrease of the scale; the original recipe was described for over 100 g of the compound and required over 10 l vessels. We think that the change in the scale of the synthesis was the reason for the decrease of our yield.[19] Moreover, any deviations from the conditions described in the literature led to the dramatic decrease in the yield. Especially the pH during all extraction processes must be kept at the value of 9.0 to avoid the protonation or deprotonation of imidazole ring, which leads to the great loss of the desired product.

The fomulas of the ligand **L** and the complexes **1**, **2**, **3** are shown in Scheme I.

Crystal structures

Crystal structure of histaminol, L Histaminol crystalizes in the *P*na2$_1$ space group of the orthorhombic system. The unit cell contains four of its molecules. The imidazole derivative

[a] P. Maślewski, A. Dołęga*
Department of Inorganic Chemistry
Faculty of Chemistry, Gdansk University of Technology
11/12 Narutowicza Str., 80-233, Gdańsk, Poland
anndoleg@pg.edu.pl,
https://chem.pg.edu.pl/kchn/grupa-dolega
[b] D. Wyrzykowski
Department of General and Inorganic Chemistry,
Faculty of Chemistry, University of Gdańsk,
63 Wita Stwosza Str., 80-308 Gdańsk, Poland
[c] M. Witwicki*
Faculty of Chemistry, Wroclaw University,
14 F. Joliot-Curie Str., 50-283 Wroclaw, Poland.

Supporting information for this article is given via a link at the end of the document.

crystallized as 1-H tautomer *i.e.* 5-hydroxyethylimidazole. Each histaminol molecule participates in the formation of four intermolecular hydrogen bonds between hydroxyl groups and both nitrogens in the imidazole ring. As a result, a layer of NH···O and OH···N interactions is formed in the crystallographic *bc* plane (Fig. 1; Table 1S). This pattern is further stabilized by van der Waals interactions, OH···π as well as π···π contacts. Additionally, there are numerous CH···π interactions between the molecules sitting in the neighboring *bc* layers, which are responsible for molecular self-assembly in the crystallographic *a* direction.

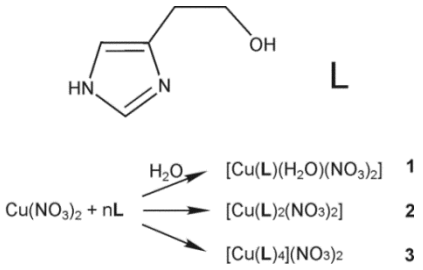

Scheme 1. Formula of the ligand **L** and complexes **1** (n=1), **2** (n=2), **3** (n=4).

Crystal structures of copper(II) – histaminol complexes

Three different copper(II) complexes with histaminol crystallized from aqueous solutions that contained different molar ratios of copper(II) nitrate and **L**. All compounds are mononuclear and Cu ions always exhibit CN = 6. Complexes **1** – **3** contain accordingly one, two and four histaminol moieties, thus illustrating successive stages of complexation process. $[CuL_3]^{2+}$ species was not isolated but it is always a minor constituent of equilibrium mixture as proved by the potentiometric titrations described in the next chapter.

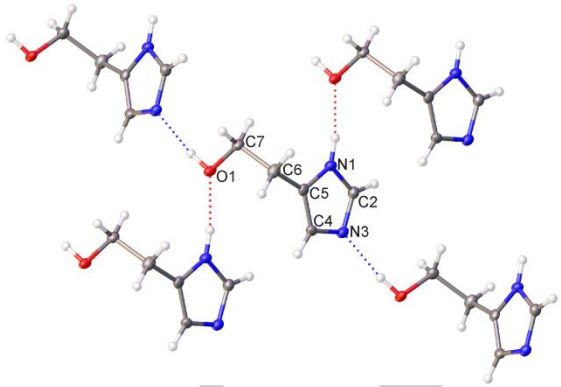

Figure 1. The molecular structure of histaminol **L** with the numbering scheme and H-bond interactions in the crystallographic *bc* plane. Displacement ellipsoids were drawn at 50% probability level.

Compound **1** $[CuL(NO_3)_2(H_2O)]$ crystalizes in the monoclinic $P2_1$ space group. As shown in Fig. 2, copper(II) is coordinated by two nitrate groups, water molecule and one chelating histaminol molecule, which binds Cu(II) via nitrogen of the imidazole ring and oxygen atom of the hydroxyl group. Coordination center contains only one metal – nitrogen bond and five metal – oxygen interactions. Complex **2** $[CuL_2(NO_3)_2]$ forms crystals in the $P2_1/c$ space group of the monoclinic crystal system. Two molecules of ligand **L** create six-membered chelate rings with the copper(II) ion, in the identical manner as the one in the complex **1** (Fig. 3). Coordination sphere is completed by two Cu–O bonds with oxygens that originate from nitrate anions. Compound **3** $[CuL_4](NO_3)_2$ crystalizes in the triclinic space group $\mathbf{P\bar{1}}$. The charge of the cationic copper complex is balanced by two non-coordinated nitrate ions (Fig. 4). Metal ion is coordinated by four histaminol molecules, two of them act as chelating bidentate ligands and the other two as monodentate bonded to copper(II) *via* an N3 nitrogen of the imidazole ring. The latter two imidazole molecules are 5-substituted tautomers whereas all chelating imidazoles in the complexes **1** – **3** are 4-substitiuted tautomers.

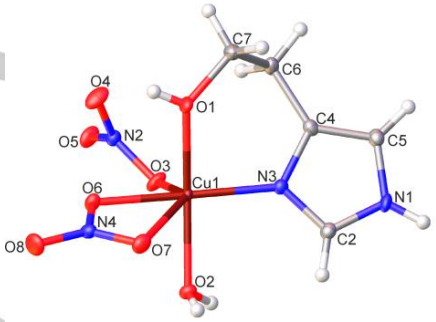

Figure 2. The molecular structure of **1** with the numbering scheme. Displacement ellipsoids were drawn at 50% probability level.

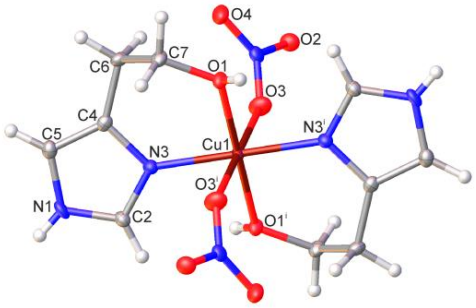

Figure 3. The molecular structure of **2** with the numbering scheme. Displacement ellipsoids were drawn at 50% probability level.

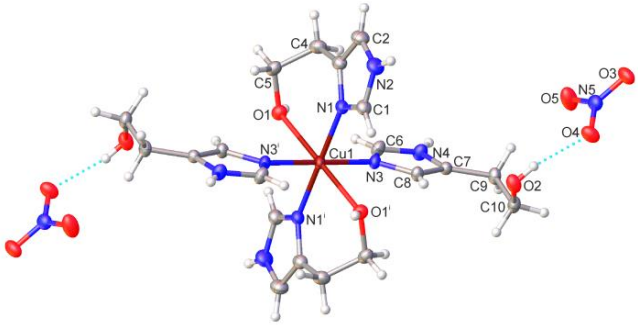

Figure 4. The molecular structure of **3** with the numbering scheme. Displacement ellipsoids were drawn at 50% probability level.

The composition of coordination centers for compounds **1** – **3** may be described as: $CuNO_5$, CuN_2O_4, CuN_4O_2. Complex **1** features rather irregular arrangement of ligands around the central atom and the deformation is primarily caused by double bonded nitrate group. It results in wide scope of angles around Cu(II) 54.51(9)° – 121.53(9)°. Moreover, distortion involves lengths of Cu1–O3 and Cu1–O7 bonds between metal atom and each of nitrates, which equal to 2.324(3) and 2.583(3) Å, respectively. Neglecting Cu1–O7 bonding the overall geometry can be reported as square pyramidal with Cu1, O1, O2, O6 and N3 forming the basal plane and nitrate O3 in the apical position. Selected interatomic bond distances and angles in the investigated complexes are listed in Table 1.

Coordination geometry for compound **2** is a slightly distorted octahedron. Two N atoms and two O atoms from chelating imidazole rings are situated on the equatorial plane and two O atoms of the nitrate groups occupy axial positions. However, the angle between Cu1–O3 bond and the plain equals 76.26(5)°. There is also tetragonal Jahn–Teller distortion in **2**; the axial bond lengths exceed the equatorial ones by 0.63Å and 0.68Å. Thus tetragonality, calculated as in ref. [20], T = 0.76. Selected molecular dimensions within the complex **2** are shown in Table 1.

Compound **3** exhibits coordination geometry around Cu(II) similar to that in **2**, however it is more regular. Bond angles in the coordination sphere are close to the value of 90° and the equatorial Cu–N bond lengths are almost equal. The axial Cu–O bonds are longer due to the Jahn–Teller effect by about 0.5Å, tetragonality T = 0.80. Equatorial bond lengths in complexes **2** and **3** and also four almost coplanar bonds in **1**, take values in the range 1.942(3) to 2.016(2) Å. Such bond distances are typical of equatorial Cu–N and Cu–O interactions in six-coordinate copper(II) complexes with imidazole derivatives, including histamine and histidine ligands.[21-31] However, degree of tetragonal distortion in such compounds is diverse and depends on composition of coordination centers.[21-31] Compounds with the CuN_4O_2 chromophore usually exhibit tetragonality T around 0.80[21,23,25,27,28], as also calculated for the complex **3**. Those with CuN_2O_4 show a wider scope of T values 0.72 – 0.86.[26,29,30]

Hydrogen bonding intermolecular interactions in crystals of complexes **1** – **3** are described in the Supporting information file (Figs. 1S - 6S, Tables 2S – 4S).

Table 1 Selected bond lengths and angles in complexes **1** - **3**

	1	**2**	**3**
	Bond lengths [Å]		
Cu1—N1	-	-	2.016(2)
Cu1—N3	1.942(3)	1.949(2)	2.015(2)
Cu1—O1	1.978(3)	1.997(2)	2.518(2)
Cu1—O2	1.992(3)	-	-
Cu1—O3	2.324(3)	2.629(2)	-
Cu1—O6	1.996(2)	-	-
Cu1—O7	2.583(3)	-	-
	Bond angles [°]		
N3—Cu1—O1/O1i	89.34(11)	91.56(5)/88.44(5)	92.14(9)/87.86
N3—Cu1—O2	93.08(11)		
O1—Cu1—O7	92.28(9)		
N3—Cu1—O7	121.53(9)		
O1—Cu1—O6	88.35(11)		
O6—Cu1—O7	54.51(9)		
O2—Cu1—O6	88.29(10)		
N3—Cu1—O3/O3i	96.09(9)	85.54(5)/94.46(5)	
O1—Cu1—O3/O3i	103.87(9)	76.26(5)/103.74(5)	
O2—Cu1—O3	88.28(13)		
O6—Cu1—O3	88.45(9)		
O2—Cu1—O7	75.8(1)		
N1—Cu1—O1			87.54 (9)
N1—Cu1—O1ii			92.46(9)
N1—Cu1—N3ii			91.42(9)
N1—Cu1—N3			88.58(9)

Potentiometric titration

The histaminol acid dissociation constant pK_a(ImH^+) and cumulative stability constants logβ_n of the complex formation between histaminol and Cu^{2+} ions are summarized in Table 2. The results are compared to the literature data of the selected imidazole derivatives. Due to the electron-donating inductive effect of hydroxyethyl group, basicity of histaminol is slightly higher in comparison to unsubstituted imidazole.[32] Impact is smaller than in the case of alkyl substituent, e.g. 4(5)-methylimidazole, since electron withdrawing hydroxyl group is present. However, the distance between nitrogen N3 atom in the imidazole ring and the hydroxyl group is too far for the electron-withdrawing effect to be dominant, contrary to 4(5)-hydroxymethylimidazole.

The obtained logβ_n values indicate that histaminol forms more stable copper(II) complexes than other C-substituted imidazole derivatives (Table 2[23,27,33-37]). Stability constants of alkylimidazoles are lower than corresponding ones for histaminol, despite their higher basicity responsible for σ-donor properties of the ligands. This can be explained by the existence of the additional interaction between the copper(II) ion and the hydroxyl group of the side chain, which enhances the stability of the complex.

Chelating ability of histaminol is confirmed by crystallographic structures presented earlier in this paper. On the other hand, hydroxymethyl and aldehyde derivatives, which are also able to chelate metal ions[36] exhibit lower basicity than histaminol which negatively influences overall stability of their complexes. The combination of chelating ability and the relatively strong basicity of histaminol makes it a strongly binding ligand.

Interestingly, the calculated logβ_n values are fairly close to the corresponding ones for 1-ethylimidazole, compound with the similar basicity. 4-Substituted tautomer of histaminol exhibits higher steric hindrance in the vicinity of the pyridine nitrogen than 1-ethylimidazole ligand, therefore this negative impact on stability seems to be totally compensated by the chelation effect.

The concentration distribution of species as a function of pH in the Cu^{2+}– histaminol system is shown in Fig. 5. The contribution of the $[CuL_3]^{2+}$ species is low and minor in the whole pH range studied. This was probably the main reason for the inability to isolate this complex, under experimental conditions, despite several attempts.

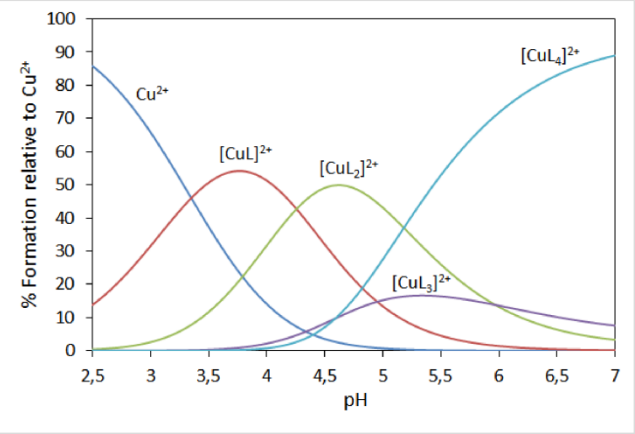

Figure 5. Concentration distribution curves of the copper(II) complexes as a function of pH calculated based on the stability constants obtained from potentiometric titration data (Table 2).

UV-Vis spectroscopy

UV-Vis titration was performed to follow the changes in electronic spectra during complexation process. The results are presented in Fig. 6. For free histaminol a single band occurs at λ_{max}=212 nm, which originates from intraligand π→π* electron transition. After binding to copper(II), this band undergoes a blue shift to λ_{max} at about 200 nm. During further titration a red shift of this band together with an increase in molar absorptivity is continuously observed, due to the rising concentration of histaminol, both bonded to metal ions and free ligand at the end of the measurement. In the UV region, two ligand to metal charge transitions (LMCT) can be observed: π_1→Cu(II) at λ range 260–320 nm, π_2→Cu(II) with λ_{max} at about 336–342 nm. Growth of the intensity of both bands become minimal after a certain point of titration when the vast majority of copper(II) ions already possess saturated coordination sphere. Another CT transition n→Cu(II) is expected at 200–220 nm, but it probably overlaps with π→π* transition. In the visible part of the spectrum a single broad band originates from metal ion *d* – *d* transition. As complexation proceeds, the band undergoes the blue shift to λ_{max} at about 600 nm, what indicates rising energy difference between molecular *d* orbitals in copper(II)–histaminol systems.[38,39]

Table 2. pK_a and logβ_n values for Cu(II)–imidazole derivatives complexes in aqueous solution at T = 298.15 K and I = 0.5 M ($NaClO_4$), standard deviations given for the values measured within this work.

Ligand	pKa	logβ1	logβ2	logβ3	logβ4	Reference
Histaminol	7.25±0.01	4.37±0.02	7.97±0.04	10.61±0.26	13.96±0.17	[this work]
Imidazole	7.12	4.31	7.84	10.76	12.90	[32]
4(5)-methylimidazole	7.80	4.18	7.74	10.70	13.05	[33]
4(5)-hydroxymethylimidazole	6.67	3.60	7.05	9.53	10.90	[34]
4-carbonyl-5-methylimidazole	4.20	3.39	5.80	7.37	8.38	[23]
1-ethylimidazole	7.25	4.40	7.99	10.98	14.20	[27]

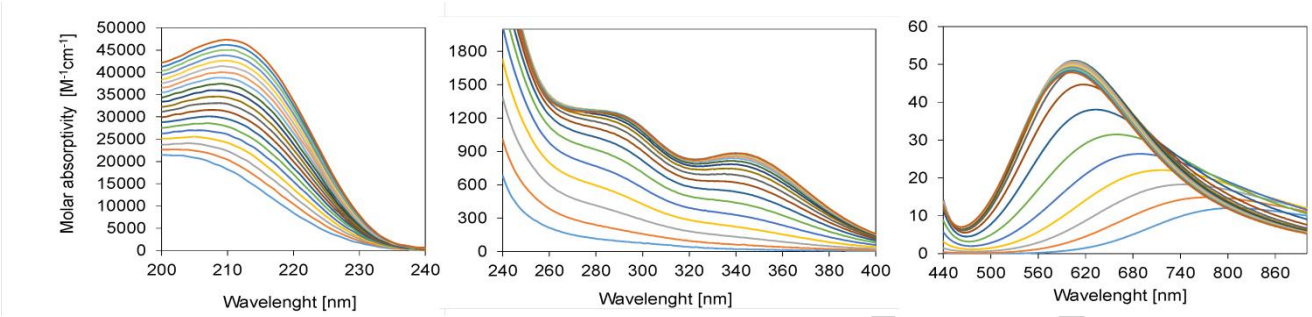

Figure 6. UV-Vis titrations of the aqueous $Cu(NO_3)_2$ solutions with the aqueous solution of histaminol for three wavelength ranges: 200–240 nm, 240–400 nm, 440–900 nm with the initial concentration of $Cu(NO_3)_2$ 0.01 mM, 0.5 mM, 10 mM respectively. Each titration was carried out to the point when the metal : ligand molar ratio exceeded 1:8.

EPR Spectroscopy

When a copper(II) ion is located in an octahedral ligand field, its 3*d* orbitals split into two sets, that is t_{2g} and e_g. Distributing nine electrons into these split orbitals places three electrons in the e_g set. The resulting electronic state is thus orbitally degenerated and unstable due to the Jahn-Teller distortion, which lifts the orbital degeneracy and lowers the molecular symmetry. If the resulting molecular structure becomes elongated octahedral, square pyramidal or square planar then the unpaired electron occupies the $d_{x^2-y^2}$ orbital and the relation between the g values is $g_z >> g_x = g_y > 2.0023$ ($g_x = g_y = g_\perp$; $g_z = g_{II}$).[40,41] The d_{z^2} orbital becomes the ground state of a Cu(II) complex, if the molecular structure is compressed octahedral or trigonal bipyramidal. In such a case the relation between the components of the g tensor is $g_x = g_y > g_z \approx 2.0023$ (so-called inversed spectrum).[40,42] In the case of intermediate situations, for instance if the geometry is between the square pyramid and the trigonal bipyramid, the EPR spectrum exhibits three different g values ($g_x < g_y < g_z$). Such a rhombic spectrum is an indication of the ground state being a linear combination of the $d_{x^2-y^2}$ and d_{z^2} orbitals.[40] A parameter G defined below:

$$G = \frac{g_y - g_x}{g_z - g_x}$$

can be used as a criterion of the predominance of the d_{z^2} or $d_{x^2-y^2}$ orbital in the ground state. If G < 1, the predominant contribution to the ground state arises from $d_{x^2-y^2}$, otherwise the greater contribution arises from d_{z^2}.[40]

EPR spectra recorded for the complexes 1 – 3 at 9.6 and 34 GHz frequencies are shown in the Figs. 7 and 8, respectively. For all the studied complexes the advantage of 34 GHz frequency (Q-band) is evident as the spectra are more fully resolved due to resonance transitions corresponding to the components of the g tensor. The components of g tensors determined from these spectra are listed in Table 4. They are in agreement with values reported previously for the Cu(II) complexes with various derivatives of imidazoles.[23,31,43,44]

Complex **1** incorporates one histaminol ligand and, according to the X-ray diffraction experiments, the Cu1–O7 distance amounts to 2.583 Å thus the coordination around the central copper metal for **1** can be approximated as slightly distorted square pyramidal for the EPR interpretation.

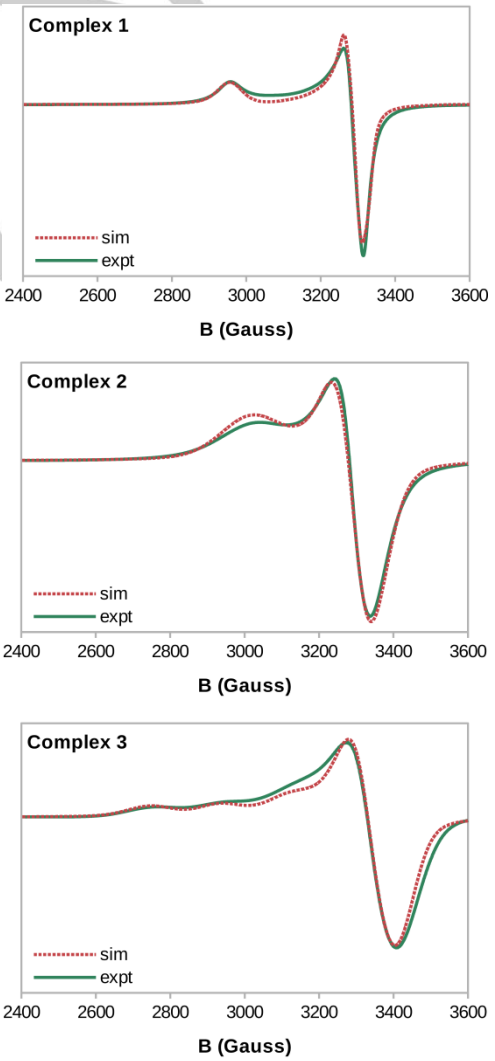

Figure 7. Experimentally recorded and simulated X-band (9.6 GHz) EPR spectra of **1**, **2** and **3**.

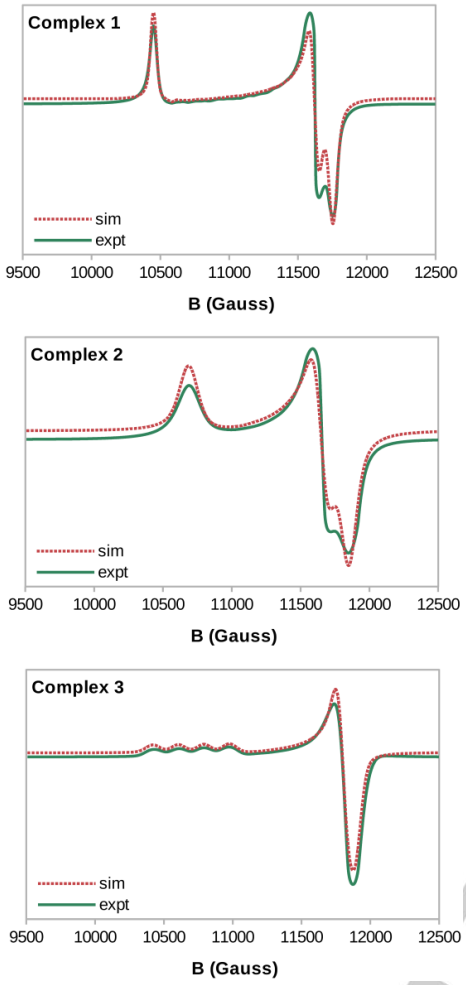

Figure 8. Experimentally recorded and simulated Q-band (34 GHz) EPR spectra of **1**, **2** and **3**.

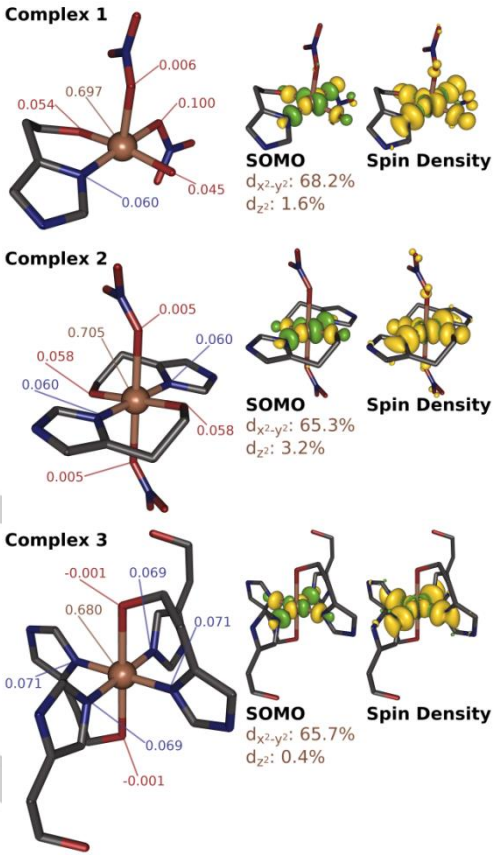

Figure 9. Loewdin spin populations, singly occupied molecular orbitals (SOMOs) contoured at ±0.05 (electrons/a_0^3)1/2, selected Loewdin reduced orbital populations and spin density distributions contoured at ±0.001 electrons/a_0^3 for complexes **1**–**3**; yellow = positive, green = negative; hydrogen atoms were removed for clarity.

The g components derived from the simulation of EPR spectra, that is g_z = 2.324, g_y = 2.090 and g_x = 2.067, are a firm indication of the d_{x2-y2} ground state with a diminutive admixture of d_{z2}. This is corroborated by the calculated parameter G = 0.089, which clearly indicates that the singly occupied molecular orbital (SOMO) of complex **1** is mainly d_{x2-y2}, but not a pure d_{x2-y2} orbital because its lobes point directly at the ligands and it is therefore prone to strong antibonding interactions with them, as predicted by the DFT calculations (Fig. 9). The B3LYP/def2-TZVP description of the ground state of complex **1** revealed that its SOMO has 68.2% d_{x2-y2} character, d_{z2} gives only 1.6% and the remaining contributions stem from the orbitals of ligands. In order to confirm that the DFT predicted ground state is correct, the g tensor for **1** was computed. Generally good agreement between the experimental and theoretical values was found indicating that the predicted electronic structure is a good illustration of the real complex. Nevertheless, the computed g_z value was clearly underestimated by the employed DFT methods.[45-47] This can be attributed to deficiencies in the calculated electronic excitation energies to the SOMO and to the overestimation of covalent bonding bringing about too significant transfer of spin density onto the ligands.[45,47]

The coordination geometry around the metal center in complex **2**, can be described as elongated octahedral with Cu(II) coordinated to two nitrogen and two oxygen donor atoms in the equatorial plane. This differentiates complex **2** from complex **1** as in the latter the central Cu atom is bonded to one nitrogen and three oxygen atoms in the equatorial plane. This significant structural difference does not change the fact that the SOMO of **2** is dominated by the contribution from the Cu d_{x2-y2} atomic orbital (G = 0.18, 65.3% according to the B3LYP/def2-TZVP calculation) but it brings about a sharp decrease in the value of g_z from 2.324 to 2.272 for **1** and **2**, respectively (Table 4). This decrease stays in line with other studies indicating that the increasing number of nitrogens in the *xy* plane of Cu lessens the g_z value, but on condition that the total charge of the coordination unit is preserved.[48] It should be noted that this trend is well reproduced in the performed DFT calculations (Table 4).

Table 4. Experimentally determined and theoretically calculated values of the g tensors components for **1** - **3**.

	1			**2**			**3**		
	g_x	g_y	g_z	g_x	g_y	g_z	g_x	g_y	g_z
X-band	2.067	2.085	2.317	2.053	2.080	2.271	2.042	2.064	2.264
Q-band	2.067	2.090	2.324	2.051	2.085	2.273	2.045	2.065	2.265
B3LYP	2.035	2.091	2.187	2.038	2.079	2.174	2.045	2.047	2.172
TPSS0	2.039	2.088	2.188	2.041	2.078	2.174	2.047	2.050	2.173

The EPR spectra of complex **3** correspond to the relation of g tensor components typical for uniaxial symmetry of the coordination sphere around Cu(II) ion, that is $g_z >> g_y = g_x > 2.002319$, in agreement with an elongated octahedral geometry of the complex determined by the X-ray crystallography. Thus, the contribution from the d_{x2-y2} atomic orbital to the SOMO is dominant (G = 0) and the DFT predictions are in accord with this finding. Although the number of nitrogen atoms in the *xy* plane of **3** is increased to 4, the g_z component undergoes only a slight decrease in comparison with complex **2**, that is from 2.273 to 2.265. This result can be explained by the fact that coordination unit in **3** is dipositively charged ($[CuL_4]^{2+}$), while in **2** it is electrically neutral ($[CuL_2(NO_3)_2]$). The increase of positive charge of the coordination unit was demonstrated to increase g_z[48], hence this effect greatly alleviates the change in g_z induced by the rising number of nitrogen atoms. The small decrease in g_z was confirmed by the DFT calculations. What stands out in the EPR spectra of **3** is the fact that they reveal fully resolved z-component of hyperfine structure to the copper nucleus (I = 3/2, $A_z = 196\times10^{-4}$ cm^{-1}), although the spectra were recorded without any dilution of the Cu(II) compound. This is a rare case that arises only if Cu(II) centers are efficiently isolated by the diamagnetic ligands and/or counter ions[23], and indeed based on the crystal structures of **1** - **3** it is evident that the shortest Cu–Cu distance in **3** is significantly longer (8.396 Å) in comparison with **1** (5.740 Å) and **2** (6.913 Å). This suggests that in the case of **3** the isotropic exchange interaction between different Cu^{2+} ions in the crystal lattice, that can be transmitted *via* intermolecular interactions, is negligible. Fig. 6S shows that there are direct contacts between the complex ions in the crystals, however imidazole ring is not directly engaged in any of these contacts (Figs. 5S and 6S). In contrast, for **1** and **2** the intermolecular interactions shown in Figs. 1S-4S might – efficiently enough - transmit the isotropic exchange interaction. Moreover this exchange interaction, although weak, might have a noticeable effect on the EPR spectral properties.[49-51] The described situation requires a cautious approach. Therefore in our study experimental g components were confirmed by the DFT calculations and their values were additionally verified by the comparison to the values found for similar Cu-imidazole systems under conditions ensuring lack of isotropic exchange interaction, namely in frozen solutions.[23,31,43,44]

Conclusions

In the paper the formation of complexes between copper(II) and histaminol (**L**) is illustrated with the X-ray diffraction structures and relevant EPR spectra. Stepwise complex formation constants are determined showing enhanced stability of the Cu-$\mathbf{L}_n$ complexes in comparison with the complexes of monodentate, C-substituted imidazoles and chelating analogues: 4-carbonyl-5-methylimidazole and 4(5)-hydroxymethylimidazole with shorter side chains. Determined pK_a of histaminol and formation constants of its complexes with Cu(II) are similar to 1-ethylimidazole. EPR spectra of $[Cu\mathbf{L}_4]^{2+}$ reveal fully resolved z-component of hyperfine structure to the copper nucleus indicating rare example of a Cu(II) center efficiently isolated by the diamagnetic ligands. UV-Vis and EPR spectra are in the complete accordance with the determined crystal structures.

Experimental Section

Synthetic procedures

All reagents needed for synthesis described below were obtained commercially and used as received.

Preparation of histaminol or 4(5)-(β-hydroxyethyl)imidazole or 4-(1H-Imidazol-2-yl)ethanol, $C_5H_8N_2O$, L Synthesis of histaminol was based on previously described method with very minor modifications.[19] It is a three-stage synthesis of: a) 1-hydroxy-4-methoxy-2-butanone **A**, b) 4(5)-(2'-methoxyethyl)imidazole **B** and finally c) **$C_5H_8N_2O$, L**:
a) 20 ml of mercury(II) sulfate solution (10 g mercury(II) sulfate, 7.5 g concentrated sulfuric acid, 67.5 ml water) was added to 450 ml of methanol. Then the solution of 150.5 g (1.75 moles) of 2 butyne-1,4-diol in 300 ml of methanol along with the rest of mercury(II) sulfate solution were slowly added as described.[19] Two additional portions of mercury(II) sulfate (1 g each) were added after 4.5 and 7 hours since the beginning of reaction. Reaction mixture was continuously stirred and the temperature was kept between 30-35°C for 9 hours. The next day 20 g of sodium carbonate was added and the obtained suspension filtered. Solution, that contained **A** was evaporated to a volume of about 250 ml and split into four equal portions.

b) Each quarter of the solution of **A** was added to 1750 ml of 12.5% aqueous ammonia solution that contained 175 g of copper(II) acetate monohydrate and 43,75 ml of 36% formaldehyde solution. The reaction mixture was stirred and heated for two and half hours at 65-75°C. After one hour of cooling in an ice bath, greenish-brown copper salt of **B** was collected. The elaboration of all parts of the solution of **A**, yielded a total of 121 g of this salt. Copper was removed by passing hydrogen sulfide through the acetic acid solution of copper salt and filtering. Solution was evaporated to a small volume, then brought to pH=9.0 (very important!) using concentrated (~10 M) solution of sodium hydroxide and extracted with 1-butanol. The butanol extracts were evaporated and the remaining oil distilled in vacuo in Kugelrohr (short-path vacuum distillation apparatus). Yield 31.5 g (0.25 moles) of 4(5)-(2'-methoxyethyl)imidazole.
c) 17.0 g (0.135 moles) of 4(5)-(2'-methoxyethyl)-imidazole were dissolved in 45 ml of 48% hydrobromic acid and refluxed for 90 minutes. Hydrobromic acid was removed by evaporation and the residue was dissolved in water. Solution was treated with the charcoal, filtered and evaporated to a small volume. Solution was brought to pH=9.0 by potassium hydroxide solution and evaporated again. Solid remnants were extracted with 1-butanol. Extract was evaporated to small volume and set to crystallization with the addition of acetone. Initially, after few days, a certain amount of a liquid phase separated at the bottom of the flask and it was removed. After subsequent ten days brownish precipitate was collected. Recrystallization from butanone provided 5,41 g (0.048 moles) of colourless crystals of 4(5)-(2'-hydroxyethyl)imidazole **L**. **Anal. Calcd.** for $C_5H_8N_2O$ (112.13): C, 53.56; H, 7.19; N, 24.98. **Found:** C, 53.11; H, 7.16; N, 24.59%. **M.p.** 88 °C. **^{1}H-NMR** (400 MHz, CH_3OD, 298 K): δ = 7.59 (s, 1H, C2-H), 6.85 (s, 1H, C5-H) 4.98 (s, 1H, O1-H), 3.78 (t, $^3J_{HH}$ = 6.9 Hz, 2H, C7-H), 2.81 (t, $^3J_{HH}$ = 7.0 Hz, 2H, C6-H) ppm. **^{13}C{1H}-NMR** (100.6 MHz, CH_3OD, 298 K): δ = 134.4 (s, C5), 133.9 (s, C2), 117.1 (s, C4), 61.2 (s, C7), 29.7 (s, C6) ppm. IR (solid): $\tilde{\nu}$ = 3115 (vs), 2994 (vs), 2959 (vs), 2905 (vs), 2838 (vs), 2771 (vs), 2559 (m), 2100 (vw), 1645 (w), 1592 (m), 1465 (m), 1435 (s), 1419 (s), 1380 (m), 1338 (m), 1258 (m), 1236 (w), 1191 (w), 1144 (vw), 1102 (s), 1073 (vs), 1026 (s), 957 (vw), 938 (m), 860 (m), 823 (s), 781 (s), 689 (w), 655 (s), 626 (w), 490 (w) cm^{-1}. UV-Vis λ_{max}=212 nm.

Preparation of complex 1 $[Cu(C_5H_8N_2O)(NO_3)_2(H_2O)]$ or $[CuL(NO_3)_2(H_2O)]$ $Cu(NO_3)_2{\cdot}3H_2O$ (0.5 mmol, 0.120 g) and histaminol (0.5 mmol, 0.056 g) were dissolved separately in methanol (5 ml for each). Both solutions were combined and the resulting solution was heated and stirred for 1 hour. It was left at room temperature for crystallization by solvent evaporation. Green crystals of complex **1** were obtained after eight weeks. **Yield** 0.088 g (55.4%). **Anal. Calcd.** for $CuC_5H_{10}N_4O_8$ (317.70): C, 18.90; H, 3.17; N, 17.64. **Found:** C, 19.11; H, 3.26; N, 17.78%. **M.p.** 97 °C. **IR + FIR (solid):** $\tilde{\nu}$ = 3266 (vs), 3139 (vs), 2947 (s), 2919 (s), 2894 (s), 1723 (vw), 1596 (w), 1507 (s), 1447 (s), 1427 (s), 1355 (m), 1307 (vs), 1273 (vs), 1185 (s), 1099 (m), 1067 (w), 1034 (m), 1016 (s), 939 (vw), 867 (w), 820 (w), 803 (m), 758 (m), 706 (w), 622 (m), 509 (w), 421 (vw), 365 (w), 330 (w), 294 (vw), 243 (vw), 224 (w), 191 (w) cm^{-1}.

Preparation of complex 2 $[Cu(C_5H_8N_2O)_2(NO_3)_2]$ or $[CuL_2(NO_3)_2]$ Complex **2** was prepared as described for complex **1** with the use of $Cu(NO_3)_2{\cdot}3H_2O$ (0.5 mmol, 0.120 g) and histaminol (1 mmol, 0.112 g). Blue-green crystals of **2** were obtained after four weeks. Yield 0.121 g (58.8%). **Anal. Calcd.** for $CuC_{10}H_{16}N_6O_8$ (411.82): C, 29.16; H, 3.92; N, 20.41. **Found:** C, 28.84; H, 3.98; N, 19.76%. **M.p.** 151 °C. **IR + FIR (solid)**: $\tilde{\nu}$ = 3341 (vs), 3154 (vs), 3134 (s), 3061 (s), 2973 (s), 2906 (s), 2861 (s), 2745 (s), 2431 (w), 1744 (vw), 1592 (m), 1506 (w), 1472 (w), 1455 (w), 1387 (vs), 1354 (s) 1296 (vs), 1276 (vs), 1240 (vs), 1227 (vs), 1187 (m), 1159 (s), 1080 (s), 1022 (s), 952 (m), 938 (w), 859 (m), 824 (m), 794 (m), 735 (s), 706 (m), 649 (vw), 622 (s), 528 (w), 422 (w), 368 (w), 347 (w), 310 (vw), 232 (w), 173 (w) cm^{-1}.

Preparation of complex 3 $[Cu(C_5H_8N_2O)_4](NO_3)_2$ or $[CuL_4](NO_3)_2$ Complex **3** was prepared as described for complex **1** with the use of $Cu(NO_3)_2{\cdot}3H_2O$ (0.5 mmol, 0.120 g) and histaminol (2 mmol, 0.224 g). Violet-blue crystals of complex **3** were obtained after eight weeks. **Yield** 0.085 g (26.8%). **Anal. Calcd.** for $CuC_{20}H_{32}N_{10}O_{10}$ (636.08): C, 37.76; H, 5.07; N, 22.02. **Found:** C, 37.66.11; H, 5.10; N, 21.86%. **M.p.** 137 °C. IR **+ FIR (solid):** $\tilde{\nu}$ = 3146 (vs), 3030 (s), 2938 (s), 2911 (s), 2888 (s), 1757 (vw), 1670 (vw), 1591 (m), 1574 (w), 1549 (vw), 1503 (m), 1476 (m), 1453 (s), 1421 (s), 1398 (m), 1340 (vs), 1317 (vs), 1271 (s), 1186 (m), 1110 (m), 1091 (w), 1065 (m), 1044 (m), 1018 (s), 969 (w), 946 (w), 931 (w), 857 (m), 819 (m), 770 (w), 655 (m), 638 (m), 620 (m), 497 (w), 349 (vw), 330 (w), 309 (vw), 282 (w), 266 (w), 177 (w) cm^{-1}.

Physicochemical methods

Potentiometric Titration (PT) Potentiometric titrations were performed in 30 mL thermostated (298.15 ± 0.10 K) cell using Cerko Lab System microtitration unit fitted with 5-mL Hamilton's syringe (syringe calibration constant k = 4.15), pH combined electrode (Schott – BlueLine 16 pH type) and a self-made measuring cell equipped with magnetic stirrer. The temperature was controlled using the Lauda E100 circulation thermostat. The electrode was calibrated according to IUPAC recommendations.[52] The composition of the titrant solution used in the experiments was as follows: 1 mM $Cu(NO_3)_2$, 4 mM histaminol and 6 mM HNO_3 (ionic strength I = 500 mM $NaClO_4$). The solutions (V_o = 5.0 mL) were potentiometrically titrated with the standardized 30 mM NaOH solution in the pH range from 2.5 to 7. The titrant was added to the titrand in increments of 0.02 mL, with a pause of 120 s. Each titration was repeated at least three times in order to check the reproducibility of the data. The stability constants of the complexes were determined using the CVEQUID program[53] by minimization of the differences between the theoretical model and the experimental data, according to Gauss-Newton-Marquart for nonlinear equations (see ref.[54] for more details). Theoretical model is presented in the Supporting information file in the Table 5S. The concentration distribution of various complex species existing in the solution as a function of pH was obtained using the HySS program.[55]

X-Ray Diffraction Single crystal X-ray diffraction data of the ligand **L** and the copper(II) complexes **1** - **3** were collected at 120(2) K on a Stoe IPDS-2T diffractometer with graphite-monochromated Mo-Kα radiation. Crystals were cooled using a Cryostream 800 open flow nitrogen cryostat (Oxford Cryosystems). Data collection and image processing was performed with X-Area 1.75 (STOE & Cie GmbH, 2015).[56] Intensity data were scaled with LANA (part of X-Area) in order to minimize differences of intensities of symmetry-equivalent reflections (multi-scan method). Structures were solved by direct methods and all non-hydrogen atoms were refined with anisotropic displacement parameters by full-matrix least squares procedure based on F2 using the SHELX–2014 program package.[57] The Olex[58] and Wingx[59] program suites were used to prepare the final version of CIF files. Olex[58] and Mercury[60] were used to prepare the figures. Hydrogen atoms were usually refined using isotropic model with U_{iso}(H) values fixed to be 1.5 times U_{eq} of C atoms for $–CH_3$ or 1.2 times U_{eq} for $–CH_2$, –NH and –CH groups. Unless the refinement was unstable, the NH and OH hydrogen atoms were refined without constraints. A summary of crystallographic data is shown in Table 1. CCDC 1569451-1569454 contain the supplementary crystallographic data for this paper. These data can be obtained free of charge from The Cambridge Crystallographic Data Centre.

EPR Spectroscopy The EPR spectra of polycrystalline complexes **1** - **3** were recorded at 9.6 GHz (X-band) and 34 GHz (Q-band) frequencies using a Bruker Elexsys E500 spectrometer equipped with a NMR teslameter and a frequency counter. The X-band spectra were recorded

at 77 K and the Q-band spectra at 298 K. The simulations of the experimental spectra were performed using a computer program employing full diagonalization of the spin Hamiltonian matrix written by A. Ozarowski (National High Magnetic Field Laboratory, Florida State University). In order to support EPR measurements DFT calculations were carried out with the ORCA 4.0.0 suite of programs.[61] In all the calculations the def2-TVZP basis set was used.[62] The structures determined from the X-ray diffraction experiments, that is $[CuL(NO_3)_2(H_2O)]$, $[CuL_2(NO_3)_2]$ and $[CuL_4]^{2+}$ for **1**, **2** and **3**, respectively, were used in the calculations, but only after the positions of all hydrogen atoms were optimized with the hybrid functional B3LYP.[63-65] The g tensor calculations were performed using the coupled perturbed method[66,67] at the B3LYP and TPSS0 theory level. TPSS0 stands for the hybrid version of the meta-GGA functional TPSS with 25% of HF exchange.[68,69] The combination of the TZVP-type basis set and hybrid functionals has been shown to be accurate in prediction of spin distribution and g tensors.[70-74]

Other Physico-Chemical Measurements UV-Vis measurements were carried out using the Perkin-Elmer Lambda 650 instrument equipped with the Temperature Control – Peltier System with a scan accuracy of 1 nm and 1 nm aperture width at a 120.00 nm min^{-1} scanning rate. Titrations were performed in 5 mL cuvette using Cerko Lab System microtitration unit fitted with 5-mL Hamilton's syringe (syringe calibration constant k = 4.15) at the temperature 298.15 ± 0.10 K. Aqueous solution (V_o = 2.2 mL) of copper(II) nitrate was titrated with aqueous solution of histaminol. The titrant was added in increments of 0.04 mL, with a pause of 300 s. Titrations were conducted separately for three wavelength ranges: 200–240 nm, 240–400 nm, 440–900 nm. Initial concentration of copper(II) ions/histaminol was accordingly 0.01 mM/0.25 mM, 0.5 mM/12 mM, 10 mM/250 mM. Each titration was carried out to the point when metal : ligand molar ratio exceeded 1:8. Spectrum of free ligand was measured for 0.04 mM aqueous solution.

The elemental analyses (C, H, S and N contents) were performed on an Elemental Analyser Vario El Cube CHNS (Elementar). The ^{1}H NMR and ^{13}C NMR spectra in CD_3OD were registered at 400 MHz Bruker Avance III spectrometer. The solid state IR spectra were measured using Nicolet iS50 FT-IR spectrometer equipped with the Specac Quest single-reflection diamond attenuated total reflectance (ATR) accessory controlled by Omnic computer software in range 4000–400 cm^{-1}.

Table 1 Selected crystallographic parameters for **L** and complexes **1** – **3**.

	L	**1**	**2**	**3**
Empirical formula	$C_5H_8N_2O$	$C_5H_{10}CuN_4O_8$	$C_{10}H_{16}CuN_6O_8$	$C_{20}H32CuN10O10$
Formula weight	112.13	317.71	411.83	636.09
Temperature [K]	120(2)	120(2)	120(2)	120(2)
Wavelength [Å]	0.71073	0.71073	0.71073	0.71073
Crystal system	Orthorhombic	Monoclinic	Monoclinic	Triclinic
Space group	P na21	P 21	P 21/c	P -1
Unit cel dimensions:				
a [Å]	8.4767(6)	7.706(5)	8.1098(15)	8.396(7)
b [Å]	13.1114(10)	9.128(9)	10.650(2)	8.876(8)
c [Å]	4.908(2)	8.699(6)	8.8171(16)	9.783(9)
α [°]	90	90	90	82.75(7)
β [°]	90	116.23(5)	101.334(15)	72.38(7)
γ [°]	90	90	90	75.82(7)
V [$Å^3$]	545.5(2)	548.8(8)	746.7(2)	672.6(10)
Z	4	2	2	1
Calculated density [Mg/m3]	1.365	1.923	1.832	1.570
Absorption coefficient [mm-1]	0.098	2.034	1.522	0.885
F(000)	240	322	422	331
Crystal size [mm]	0.40×0.25×0.10	0.21×0.16×0.11	0.29×0.20×0.14	0.09×0.07×0.06
Theta range for data collection	4.434 – 25.980	3.435 – 25.999	3.661 – 25.999	3.851 – 29.164
Limiting indices	-10 ≤ h ≤ 10; -16 ≤ k ≤14; 6 ≤ l ≤ 5	-9 ≤ h ≤ 9; -11 ≤ k ≤11; -10 ≤ l ≤ 10	-10 ≤ h ≤ 10; -13 ≤ k ≤13; -10 ≤ l ≤ 9	-11 ≤ h ≤ 11; -12 ≤ k ≤12; -13 ≤ l ≤ 13
Reflections collected / unique	2735 / 899	12408 / 2166	4433 / 1463	20527 / 3615
R(int)	0.0283	0.0349	0.0393	0.0481
Data / restraints / parameters	899 / 1 / 82	2166 / 1 / 175	1463 / 0 / 123	3615 / 0 / 203
Goodness-of-fit on F2	1.064	1.004	1.023	1.036
Final R indices [I>2σ(I)]	R1 = 0.0236; wR2 = 0.0626	R1 = 0.0185; wR2 = 0.0455	R1 = 0.0236; wR2 = 0.0624	R1 = 0.0341; wR2 = 0.0728
R indices (all data)	R1 = 0.0241; wR2 = 0.0629	R1 = 0.0196; wR2 = 0.0458	R1 = 0.0294; wR2 = 0.0638	R1 = 0.0493; wR2 = 0.0774
Absolute structure parameter	-0.1(7)	0.018(9)	-	-
Largest diff. peak and hole [e·$Å^{-3}$]	0.169; -0.149	0.264; -0.237	0.372; -0.322	0.377; -0.447

Keywords: Copper • Histaminol • X-ray diffraction • EPR Spectroscopy • Stability constants

[1] M. Jutel, T. Watanabe, M. Akdis, K. Blaser, C. A. Akdis, *Curr Opin Immunol.* **2002**, *14*, 735-740.
[2] C. A. Akdis, K. Blaser, *J. Allergy Clin. Immunol.* **2003**, *112*, 15-22.
[3] P. Górski, *Alergia* **2007**, *4*, 33-35.
[4] G. Kastas, H. Pasaoglu, B. Karabulut, *Polyhedron* **2011**, *30*, 2599-2605.
[5] D. Mikulski, K. Basinski, A. Gasowska, R. Bregier-Jarzebowska, M. Molski, L. Lomozik, *Polyhedron* **2012**, *31*, 285-293.
[6] G. Marone, F. Granata, G. Spadaro, A. Genovese, M. Triggiani. *J. Allergy Clin. Immunol.* **2003**, *112*, S83-S88.
[7] J. Bergmark, G. Granerus, *Scand. J. Clin. Lab. Invest.* **1974**, *34*, 365-373.
[8] M. Bordiga, F. Travaglia, M. Locatelli, M. Arlorio, J. D. Coisson, *J. Agric. Food Chem.* **2010**, *58*, 10202-10208.
[9] E. López-Rituerto, A. Avenoza, J. H. Busto, J. M. Peregrina, *J. Agric. Food Chem.* **2013**, *61*, 9464-9469.
[10] Z. Tarnok, I. Tarnok, *Agents Actions* **1986**, *18*, 1–2.
[11] I. Bertini, A. Rosato, *Eur. J. Inorg. Chem.* **2007**, *18*, 2546-2555.
[12] C. Andreini, I. Bertini, A. Rosato, *Acc. Chem. Res.* **2009**, *42*, 1471-1479.
[13] T. Gajda, B. Henry, J.-J. Delpuech, *J. Chem. Soc. Dalton Trans.* **1993**, 1301-1306.
[14] C. E. Elwell, N. L. Gagnon, B. D. Neisen, D. Dhar, A. D. Spaeth, G. M. Yee, W. B. Tolman, *Chem. Rev.* **2017**, *117*, 2059-2107.
[15] P. Garnuszek, J. K. Maurin, J. Witowska-Jarosz, B. Ptasiewicz-Bąk, *Inorg. Chim. Acta* **2002**, *338*, 119-126.
[16] J. J. Bonnet, J. A. Ibers, *J. Am. Chem. Soc.* **1973**, *95*, 4829–4833.
[17] A. Torreggiani, M. Tamba, S. Bonora, G. Fini, *Biopolymers* **2003**, *72*, 290-298.
[18] S. Materazzi, R. Curini, A. Gentili, G. D'Ascenzo, *Thermochim. Acta* **1997**, *307*, 45-50.
[19] W. Bloemhoff, K. E. T. Kerling, *Recl. Trav. Chim. Pays-Bas* **1970**, *89*, 1181-1184.
[20] R. J. Dudley, B. J. Hathaway, P. G. Hodgson, *J. Chem. Soc. A* **1971**, 3355-3358.
[21] N. Camerman, J. K. Fawcett, T. P. A. Kruck, B. Sarkar, A. Camerman, *J. Am. Chem. Soc.* **1978**, *100*, 2690-2693.
[22] T. Ono, Y. Sasada, *Bull. Chem. Soc. Jpn.* **1981**, *54*, 90-93.
[23] B. Barszcz, T. Głowiak, J. Jezierska, *Polyhedron* **1999**, 18, 3713-3721.
[24] F. B. Stocker, P. Fadden, S. Dreher, D. Britton, *Inorg. Chem.* **1999**, *38*, 3251-3253.
[25] C.-G. Zhang, C.-Y. Duan, Q. Hu, D.-Y. Yan, *J. Chem. Crystallogr.* **1999**, *29*, 1153-1155.
[26] K. S. Min, M. P. Suh, *J. Solid State Chem.* **2000**, *152*, 183-190.
[27] K. Kurdziel, T. Głowiak, J. Jezierska, *Polyhedron* **2002**, *21*, 1857-1863.
[28] G. Facchin, M. H. Torre, E. Kremer, E. J. Baran, A. Mombrú, H. Pardo, M. P. Araujo, A. A. Batista, A. J. Costa-Filho, *Inorg. Chim. Acta* **2003**, *355*, 408-413.
[29] E. Shimizu, M. Kondo, Y. Fuwa, R. P. Sarker, M. Miyazawa, M. Ueno, T. Naito, K. Maeda, F. Uchida, *Inorg. Chem. Commun.* **2004**, 7, 1191-1194.
[30] L.-Z. He, S.-J. Li, W.-D. Song, D.-L. Miao, *Acta Crystallogr. Sect. E Struct. Rep. Online* **2010**, 66, m896.
[31] S. Godlewska, J. Jezierska, K. Baranowska, E. Augustin, A. Dołęga, *Polyhedron* **2013**, *65*, 288-297.
[32] G. Berton, C. Luca, *Anal. Chim. Acta* **1970**, *51*, 239-248.
[33] B. Lenarcik, K. Obłąk, Ann. Soc. Chim. Polonorum (Roczniki Chem.) **1977**, 51, 2079-2087.
[34] J. Kulig, J. Kurdziel, B. Barszcz, B. Lenarcik, *Pol. J. Chem.* **1991**, *65*, 2159-2167.
[35] B. Lenarcik, P. Ojczenasz, *J. Heterocyclic Chem.* **2002**, *39*, 287-290.
[36] B. Barszcz, *Coord. Chem. Rev.* **2005**, *249*, 2259-2276.
[37] E. Radzyminska-Lenarcik, *Sep. Sci. Technol*. **2009**, *44*, 954-970.
[38] E. Bernarducci, P. K. Bharadwaj, K. Krogh-Jespersen, J. A. Potenza, H. J. Schugar, *J. Am. Chem. Soc.* **1983**, 105, 3860-3866.
[39] E. Bernarducci, W. F. Schwindinger, J. L. Hughey IV, K. Krogh-Jespersen, H. J. Schugar, *J. Am. Chem. Soc.* **1981**, 103, 1686-1691.
[40] B. J. Hathaway, D. E. Billing, *Coord. Chem. Rev.* **1970**, *5*, 143–207.
[41] E. I. Solomon, *Inorg. Chem.* **2006**, *45*, 8012–8025.
[42] J. Jezierska, J. B. Raynor, *J. Chem. Soc. Dalton Trans*. **1981**, 56–60.
[43] R. P. Bonomo, F. Riggi, A. J. Di Bilio, *Inorg. Chem.* **1988**, *27*, 2510–2512.
[44] P. Comba, N. Dovalil, G. R. Hanson, J. R. Harmer, C. J. Noble, M. J. Riley, B. Seibold, *Inorg. Chem.* **2014**, *53*, 12323–12336.
[45] F. Neese, *Magn. Reson. Chem.* **2004**, *42*, S187–S198.
[46] A. Giard, B. Xerri, I. Ciofini, D. Berthomieu, *Chem. Phys. Lett.* **2014**, *614*, 226–233.
[47] S. Kumar, R. P Sharma, P. Venugopalan, M. Witwicki, V. Ferretti, *J. Mol. Struct.* **2016**, *1123*, 124–132.
[48] J. Peisach, W. E. Blumberg, *Arch. Biochem. Biophys.* **1974**, *165*, 691–708.
[49] K. Hoffmann, W. Hilczer, J. Goslar, *Appl. Magn. Reson.* **1994**, *7*, 289-321.
[50] R. Calvo, *Appl. Magn. Reson.* **2007**, *31*, 271-299.
[51] A. C. Rizzi, N. I. Neuman, P. J. González, C. D. Brondino, *Eur. J. Inorg. Chem.* **2016**, 192–207.
[52] I. Brandariz, J. Barriada, T. Vilarino, M. S. de Vicente, *Monatsh. Chem.* **2004**, *135*, 1475-1488.
[53] J. Kostrowicki, A. Liwo, *Comput. Chem.* **1987**, *11*, 195-210.
[54] J. Kostrowicki, A. Liwo, *Talanta*. **1990**, *37*, 645-650.
[55] L. Alderighi, P. Gans, A. Ienco, D. Peters, A. Sabatini, A. Vacca, *Coord. Chem. Rev.* **1999**, *184*, 311-318.
[56] STOE & Cie GmbH, X-Area 1.75, software package for collecting single-crystal data on STOE area-detector diffractometers, for image processing, scaling reflection intensities and for outlier rejection; **2015**, Darmstadt.
[57] G. M. Sheldrick, *Acta Crystallogr. Sect. C: Struct. Chem.* ***2015***, *71*, 3-8; G. M. Sheldrick, SHELXL-2014. **2014**, University of Göttingen and Bruker AXS: Karlsruhe, Germany.
[58] O. V. Dolomanov, L. J. Bourhis, R. J. Gildea, J. A. K. Howard, H. Puschmann, *J. Appl. Cryst.* **2009**, *42*, 339-341.
[59] L. J. Farrugia, *J. Appl. Crystallogr.* **2012**, *45*, 849-854.
[60] C. F. Macrae, P. R. Edgington, P. McCabe, E. Pidcock, G. P. Shields, R. Taylor, M. Towler, J. van de Streek, *J. Appl. Cryst.* **2012**, *45*, 849-854.
[61] F. Neese, *Wiley Interdiscip. Rev. Comput. Mol. Sci.* **2012**, *2*, 73–78.
[62] F. Weigend, R. Ahlrichs, *Phys. Chem. Chem. Phys.* **2005**, *7*, 3297–3305.
[63] A. D. Becke, *J. Chem. Phys.* **1993**, *98*, 5648–5652.
[64] C. Lee, W. Yang, R. G. Parr, *Phys. Rev. B* **1988**, *37*, 785–789.
[65] P. J. Stephens, F. J. Devlin, C. F. Chabalowski, M. J. Frisch, *J Phys. Chem.* **1994**, *98*, 11623–11627.
[66] F. Neese, *J. Chem. Phys.* **2005**, *122*, 34107–34112.
[67] F. Neese, *J. Chem. Phys.* **2001**, *115*, 11080–11096.
[68] M. M. Quintal, A. Karton, M. A. Iron, A. D. Boese, J. M. L. Martin, *J. Phys. Chem. A* **2006**, *110*, 709–716.
[69] J. Tao, J. P. Perdew, V. N. Staroverov, G. E. Scuseria, *Phys. Rev. Lett.* **2003**, *91*, 146401.
[70] A. Kochem, T. Weyhermüller, F. Neese, M. van Gastel, *Organometallics* **2015**, *34*, 995–1000.
[71] F. Neese, *Coord. Chem. Rev.* **2009**, *253*, 526–563.
[72] M. Witwicki, *ChemPhysChem* **2015**, *16*, 1912–1925.
[73] M. Witwicki, J. Jezierska, *J. Phys. Chem. B* **2011**, *115*, 3172–3184.
[74] M. Witwicki, J. Jezierska, *Theor. Chem. Acc.* **2013**, *132*, 1383-1396.

Entry for the Table of Contents

FULL PAPER

Histaminol **L** is found in nature as a metabolite of histamine. Its pK_a value is reported and the formation of complexes between Cu(II) and histaminol in aqueous solution is characterized by stepwise stability constants. The molecular structures of [Cu**L**$(H_2O)(NO_3)_2$], [Cu$\mathbf{L}_2(NO_3)_2$] and [Cu$\mathbf{L}_4](NO_3)_2$ are determined by X-ray diffraction and for all species solid state EPR spectra are analyzed.

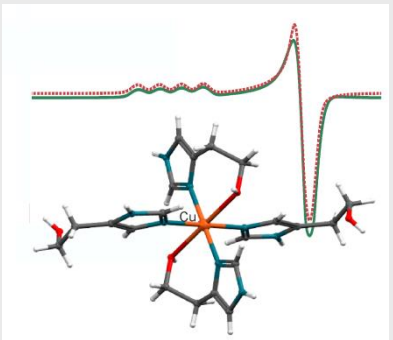

Copper - Histaminol Complexes

*Piotr Maślewski, Dariusz Wyrzykowski, Maciej Witwicki, Anna Dołęga**

Page No. – Page No.

Histaminol and its complexes with copper(II) – studies in solid state and solution